Internal transitions of confined neutral magnetoexcitons in GaAs/Al$_x$Ga$_{1-x}$As quantum wells

H. A. Nickel,[1] G. Kioseoglou,[1] T. Yeo,[1] H. D. Cheong,[1] A. Petrou,[1] B. D. McCombe,[1] D. Broido,[2] K. K. Bajaj,[3]
and R. A. Lewis[4]

[1]*Department of Physics and Center for Advanced Photonic and Electronic Materials,*
State University of New York at Buffalo, Buffalo, New York 14260
[2]*Department of Physics, Boston College, Chestnut Hill, Massachusetts 02167*
[3]*Department of Physics, Emory University, Atlanta, Georgia 30322*
[4]*Department of Physics, University of Wollongong, Wollongong NSW, Australia*

Optically detected resonance spectroscopy has been used to study resonant absorption of electrons, holes, and their complexes in GaAs/Al$_x$Ga$_{1-x}$As quantum wells (QW's) in magnetic fields up to 15 T. In undoped multiple-QW samples with well widths of 12.5, 15, and 20 nm, in addition to an electron and two hole cyclotron resonances, $1s \rightarrow np_{+,-}$ (in the hydrogenic notation) internal exciton transitions (IET's) arising from two distinct neutral heavy-hole magneto-excitons were observed. The unique capability of observing electron and hole cyclotron resonance as well as several IET's in a single sample permitted verification of a predicted relationship resulting from the symmetry of the magnetoexciton Hamiltonian, namely, $\hbar(\omega_e - \omega_h) = E_{1s\text{-}np_+} - E_{1s\text{-}np_-}$, where $\omega_e(\omega_h)$ is the electron (hole) cyclotron frequency, and $E_{1s\text{-}np_+}$ ($E_{1s\text{-}np_-}$) is the energy of the $1s \rightarrow np_+$ ($1s \rightarrow np_-$) transition.

I. INTRODUCTION

In semiconductor quantum-well structures that confine charge carriers strongly, a series of quasi-two-dimensional (2D) excitons exists corresponding to the various interband transitions between confined electron and hole subbands.[1] Such neutral excitons have been studied in a number of different materials systems for many years, predominantly by photoluminescence, absorption (and photoluminescence excitation spectroscopy), and reflectivity.[2,3] Excited states of neutral excitons are connected to the ground state by electric-dipole transitions satisfying the usual selection rules, e.g., s to np in the three-dimensional hydrogenic notation at zero magnetic field.[4] At low magnetic fields these energy levels and transition energies are only slightly modified by the magnetic ''perturbation,'' leading to the usual Zeeman splittings. At very high magnetic fields, however, the magnetoexciton states are more suitably described by considering the Coulomb interaction to be a perturbation on the high field free-carrier (electron and hole) Landau oscillator states. In this limit for each subband there is an excitonic state associated with each electron and hole Landau level, and the intraexcitonic transitions can be considered to be Coulomb-shifted electron cyclotron resonance (CR) (evolving from the $1s \rightarrow 2p_+$ low field transition) and Coulomb-shifted hole CR (evolving from the $1s \rightarrow 2p_-$ transition). Here the subscript $\pm$ denotes the quantum number ($m_z = \pm 1$) for projection of orbital angular momentum of the relative motion, and the spectroscopic notation has been used. The transition energy is blueshifted from the corresponding CR energy in each case.

Despite the abundance of interband studies of excitons in various semiconductor quantum-well systems, which generally probe only s states,[5] very little work has been done on internal transitions,[6] which probe the p-like excited states. The hydrogenic exciton system in semiconductors is superficially very similar to its close relative, the hydrogenic donor. However, the fundamental difference, namely, the mo-

bility of the hole and the center of mass of the exciton, leads to a different relationship between the energies of certain internal transitions and the cyclotron resonance energies,[7] as discussed below. The internal transitions offer an additional tool for understanding the excitonic state in the dilute situation and its evolution with excess electron density and magnetic field.[8–10] For the high exciton density situation it may also provide the possibility to probe exciton-exciton interactions and the signature of an exciton condensate.

Over the past 10 years a new type of optical detection technique has been developed and used by a number of groups for investigation of CR and other transitions in bulk[11–13] and quasi-2D semiconductor structures[14–16] in the far-infrared (FIR), or terahertz, region of the spectrum. Generally, with this technique one monitors changes in the photoluminesence, which are induced by resonant absorption of FIR radiation. This technique possesses several significant advantages over conventional FIR techniques. In addition to high sensitivity and resolution, the spectral specificity of both the near-IR photoluminescence (PL) lines and the FIR absorption can be utilized to gain information about various mechanisms of energy transfer. This technique was used in the first observation of internal transitions of excitons in direct-gap quantum-well (QW) structures,[17,18] and in later nonlinear studies.[19] The use of a FIR laser broadens the utility of this technique from its original implementation in the microwave region[20] and permits a wide variety of electronic excitations to be accessed and studied. This has been exploited recently in detailed studies of electron CR, and internal transitions of neutral and charged donors in GaAs quantum wells in magnetic fields.[16] In most implementations a sample is illuminated simultaneously by two beams, one visible and one in the FIR. The chopped FIR laser excites electronic transitions whose energies are tuned into resonance with the photon energy by an applied magnetic field. Resulting changes induced in the near-IR PL simultaneously excited by a visible laser having photon energy greater than the effective band gap of the structure under investigation are

synchronously detected. The changes in intensity and shape of a particular band-edge PL feature, which are induced by resonant absorption of FIR radiation, are monitored. The high sensitivity permits the detection of resonances involving very low densities of (photoexcited) free carriers and excitons in undoped structures, and impurities in intentionally doped QW's. The spectral specificity offers the possibility of obtaining detailed information about mechanisms of energy transfer from the various internal transitions excited by the FIR to the different recombination channels.

We have used optically detected resonance (ODR) spectroscopy to extend our earlier measurements on narrow quantum wells[17,7] to encompass a range of well widths, and have measured e-CR, h-CR, and internal transitions of neutral excitons over a range of magnetic fields and photon energies. These experiments permit a detailed comparison with, and verification of, the predicted symmetry-related effects, and also provide accurate measurements of the hole CR energies for transitions originating in the $N_h = 0$ Landau level (LL) of the $m_J = \pm \frac{3}{2}$ valence band.

In the following we provide a brief theoretical background emphasizing the symmetry of the Hamiltonian pertinent to discussion of the various transitions and their relationship with the cyclotron resonances (Sec. II). We follow this in Sec. III by a description of the experimental setup and a discussion of the ODR techniques. In Sec. IV we present and discuss the experimental results, and finally summarize and conclude in Sec. V.

II. THEORETICAL BACKGROUND

The Hamiltonian for a two-dimensional neutral exciton in a semiconductor with simple parabolic conduction and valence bands in a magnetic field can be written as

$$H = \frac{p_{rel}^2}{2\mu} + \frac{e^2 B^2}{8\mu c^2} r^2 - \frac{e^2}{\varepsilon r} + \frac{1}{2}(\omega_{ce} - \omega_{ch})\hat{l}_z$$

$$+ \frac{e}{Mc} \mathbf{B} \cdot [\mathbf{r} \times \mathbf{K}] + \frac{\hbar^2 K^2}{2M}, \qquad (1)$$

where μ is the reduced electron-hole mass, $M = m_e + m_h$, with $m_{e(h)}$ the electron (hole) mass, $\hat{l}_z$ is the operator for projection of the relative angular momentum along the magnetic field direction, B is the magnetic induction, r is the relative coordinate in the plane perpendicular to B, ε is the background dielectric constant, and K is the momentum of the center of mass of the exciton. The last term in Eq. (1) is associated only with the motion of the center of mass and the next-to-last term describes the coupling between the center-of-mass motion and the relative motion.[21] Magneto-PL lines are dominated by transitions with $K = 0$; at $K = 0$ the solutions to Eq. (1) are a set of discrete states that evolve from the usual hydrogenic states at low fields ($1s$, $2p_{\pm 1,0}$, $3d_{\pm 2, \pm 1, 0}$, etc. in the 3D spectroscopic notation) to high-field states associated with each electron (hole) LL.[4] In the high-field case for quasi-2D systems, the states can be labeled by the electron (hole) Landau quantum number, n_e (n_h), and $n_e - n_h$, the projection of relative angular momentum m_z. A quantum number i corresponding to the subband index is implicit. Since the projection of angular momentum
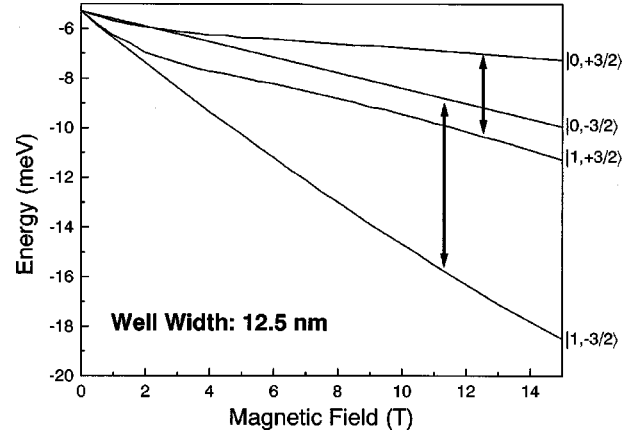

FIG. 1. Calculated Landau-level structure for holes in the valence band of a GaAs/Al$_{0.3}$Ga$_{0.7}$As QW structure with 12.5-nm wells. The parameters of the calculation are given in the text. ''Heavy-hole'' CR transitions ($N = 0 \rightarrow N = 1$) for the two spin states ($m_J = \pm \frac{3}{2}$) are indicated.

along the field direction is always a good quantum number irrespective of the strength of the magnetic field, allowed electric-dipole transitions satisfy the selection rule $\Delta m_z = \pm 1$. This neglects small warping terms in the valence band.

As a result of the cylindrical symmetry leading to Eq. (1), at $K = 0$ the following important relationship is satisfied:[7] $E_{1s \rightarrow np_+} - E_{1s \rightarrow np_-} = \hbar(\omega_{ce} - \omega_{ch})$, where $\omega_{ce(h)}$ is the electron(hole) cyclotron resonance frequency, and $E_{1s \rightarrow np_{+(-)}}$ is the transition energy from the ground state to an excited state (labeled by the 3D principal quantum number n, the total angular momentum quantum number l (in spectroscopic notation), and by the projection of relative angular momentum quantum number $m_z = \pm 1$.

The top of the valence band of GaAs is complex; in a quantum well in a magnetic field there are two optically active exciton recombination lines for the so-called heavy holes: $J = \frac{3}{2}$, $m_J = \pm \frac{3}{2}$, with J the total angular momentum and m_J its projection along an axis. The energy splittings of these two excitons in a field are directly related to splittings of the $\pm \frac{3}{2}$ hole states. This is easily seen from Fig. 1, which shows a plot of the highest hole Landau levels in the valence band for a 12.5-nm GaAs quantum well. Here the hole states are labeled $|n_h m_J\rangle$, where $n_h = n' - m_J - \frac{1}{2}$, with n' the harmonic oscillator index, and m_J the z component of total angular momentum ($J = \frac{3}{2}$). The hole wave function takes the closed form: $[F_{n'-2,3/2}, F_{n'-1,1/2}, F_{n', -1/2}, F_{n'+1, -3/2}]$. The following Luttinger parameters were used in the calculation: $\gamma_1 = 6.85$, $\gamma_2 = 2.1$, $\gamma_3 = 2.9$, and $\kappa = 1.2$. The large spin splitting of the $m_J = \pm \frac{3}{2}$ states for the $n_h = 0$ LL is apparent at high magnetic fields. The relationship between the $2p_+$ and $2p_-$ energy differences and the electron and hole energy differences holds even for these complex valence bands, as long as the Hamiltonian is cylindrically symmetric.

In this system at high fields the selection rules on m_z, the relationship $m_z = n_e - n_h$ for the lowest transitions, and the selection rule $\Delta o = 0$, with o the orbit-center quantum number ($m_z = n - o$), lead to the result that the $\Delta m_z = +1$ transitions correspond to $\Delta n_e = +1$, and the $\Delta m_z = -1$ transitions correspond to $\Delta n_h = +1$. Thus the Δm_z

$=+1$ transitions correspond to excitation of the electron from n_e to n_e+1 and the $\Delta m_z = -1$ transitions correspond to excitation of the hole from n_h to n_h+1. These results will be used later to understand the large observed splitting between the $1s \rightarrow np_-$ transitions and the lack of an observable splitting between the $1s \rightarrow np_+$ internal exciton transitions (IET's) for the two optically active magnetoexcitons.

III. EXPERIMENTAL DETAILS

The basic experimental setup for the present ODR measurements has been described previously.[16] We have recently developed a variant of this technique, reflectance ODR, which involves monitoring changes in the band-edge reflectivity features induced by resonant far-infrared absorption.[22] In the present experiments half of a SPEX Model 1401 $\frac{3}{4}$-meter instrument was used as a single grating monochromator. The energy window of the monochromator was set to encompass the desired PL feature (typical energy windows were 5 cm^{-1}). The PL signal in this spectral window was detected either with a Si photodiode or a photomultiplier detector, and a PC, controlled by a program that has been calibrated by magneto-PL spectra taken every 0.5 T, stepped the monochromator drive to track the particular PL feature(s) of interest within the energy window as the field was swept. The output signal from a lock-in amplifier (difference between the PL with FIR laser on and that with FIR laser off) is proportional to changes in intensity and/or shape of a particular band-edge PL feature, which have been induced by the absorption of FIR radiation. The visible excitation laser beam in these experiments was the 632.8-nm line from a 20- or 35-mW HeNe laser. Under normal conditions, detectable signals correspond to $\Delta I/I = 0.001$ or better; typical signals are $\sim$ of 0.01.

Three molecular-beam-epitaxy-grown, undoped GaAs/Al$_x$Ga$_{1-x}$As multiple-QW (MQW) samples were studied in this work; well widths are 12.5, 15, and 20 nm, barrier widths are 12.5, 10, and 20 nm, and $x = 0.3$, 0.15, and 0.15, respectively.

IV. EXPERIMENTAL RESULTS AND DISCUSSION

The results presented in this section extend our earlier work on IET's of neutral excitons.[17] We present experimental ODR data for three samples and compare the results for the measured IET's and electron and hole CR with theoretical calculations and with the symmetry-based relationship discussed in Sec. II.

Examples of ODR scans for sample 1 are given in Fig. 2. The upper panel shows electron CR at 1.7 T, the $m_J = -\frac{3}{2}$ hole CR at 4.3 T, and the $m_J = +\frac{3}{2}$ hole CR at 9.5 T at an FIR laser energy of 23.1 cm^{-1} ($\lambda = 432.6 \mu$m). These two principle hole CR transitions originating from the different spin states of the highest heavy-hole subband (hh1) Landau level ($|0,+\frac{3}{2}\rangle \rightarrow |1,+\frac{3}{2}\rangle$ and $|0,-\frac{3}{2}\rangle \rightarrow |1,-\frac{3}{2}\rangle$ as shown in Fig. 1) are clearly identified from circular polarization studies and comparison with the theoretical calculations described in Sec. II. The predominantly negative-going ODR signals reflect a decrease in the PL associated with the free hh$X$ caused by the CR absorption of FIR radiation. The lower trace in Fig. 2 shows several of the IET's as well as
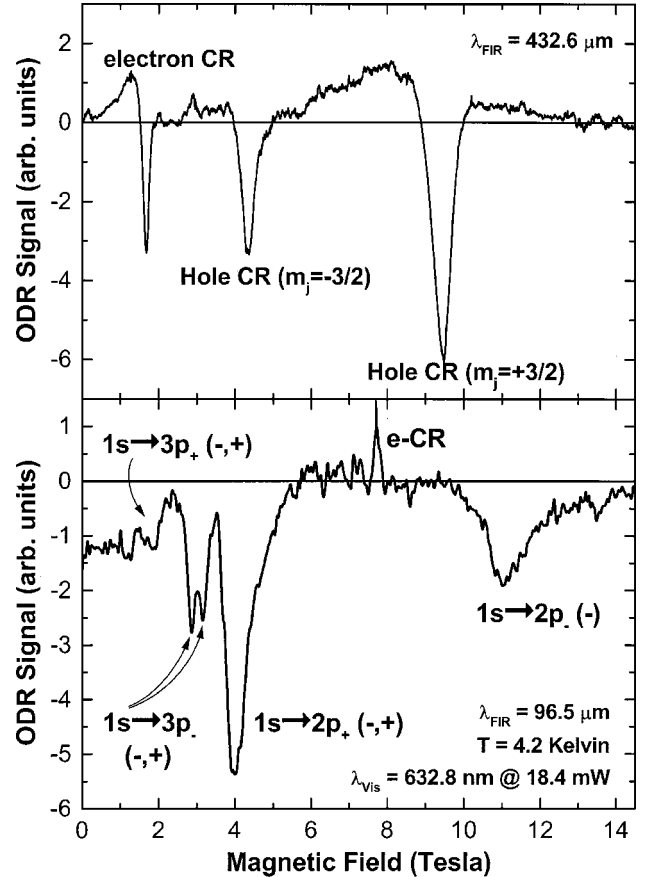

FIG. 2. ODR scans from sample 1 at 4.2 K as a function of magnetic field for FIR laser wavelengths of 432 μm (upper panel), and 96.5 μm (lower panel). IET's in the lower panel are marked with $(-)$ and /or $(+)$ to indicate the electron and hole spin states of their constituents, i.e., $(+\frac{1}{2}, -\frac{3}{2})$ or $(-\frac{1}{2}, +\frac{3}{2})$, respectively.

electron CR at 7.8 T at a FIR laser energy of 103.6 cm^{-1} ($\lambda = 96.51 \mu$m). The $1s \rightarrow 2p_+$ IET's, as well as one of the two $1s \rightarrow 2p_-$ IET's resulting from the $|+\frac{1}{2}, -\frac{3}{2}\rangle$ exciton are identified. A near degeneracy of the two $1s \rightarrow 2p_+$ transitions (over this field region) prevents observation of two individual features. Measurements with circularly polarized light at 84.2 cm^{-1} ($\lambda = 118.8 \mu$m) show that the nearly degenerate $1s \rightarrow 2p_+$ features are stronger in the electron-CR-active polarization and the $1s \rightarrow 2p_-$ features are stronger in the opposite polarization, consistent with this assignment. The near degeneracy of the $1s \rightarrow 2p_+$ features and the symmetry-derived relationship are discussed further below.

As seen in the summary plot of Fig. 3, the observed $m_J = +\frac{3}{2}$ hole CR occurs systematically about 2 cm^{-1} above the calculated position while the $m_J = -\frac{3}{2}$ hole CR agrees with the calculation to better than 1 cm^{-1}. The solid line through the electron CR data points is the result of a three-band calculation of the nonparabolicity of the conduction band on the electron LL's. The calculation ignores the resonant magneto-topolaron interaction of CR with the LO phonon at 296 cm^{-1}, which depresses the CR energy measurably at magnetic fields above about 10 T. As discussed below, the simultaneous observation of electron and hole CR in these samples along with the IET's allows the symmetry-derived relationship discussed in Sec. II to be tested. This relationship is also helpful in disentangling the complex spectrum of IET's and
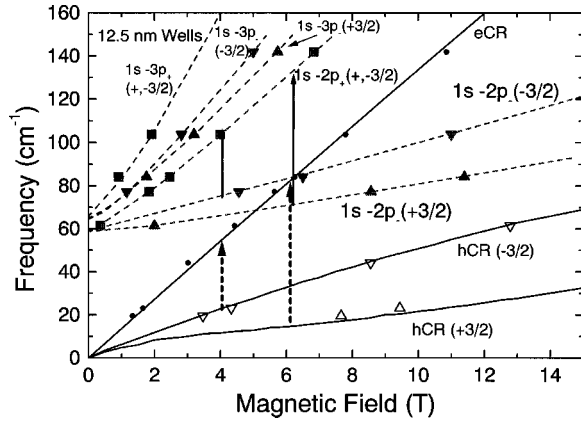
FIG. 3. Summary plot of the transition energies of the observed IET's and CR vs magnetic field for sample 1. Dashed lines are guides to the eye. Solid lines for e-CR and h-CR are calculations as described in the text. The open triangles are hole cyclotron resonances, the solid symbols represent $1s \to np_\pm$ transitions, as indicated. The lower dashed arrows show the energy difference between e-CR and h-CR$(+\frac{3}{2})$ (at 4 T) and h-CR$(-\frac{3}{2})$ (at 6 T). The upper solid arrows are the lower arrows vertically displaced to originate on the $1s \to 2p_-(+)$ transition (at 4 T) and the $1s \to 2p_-(-)$ transition (at 6 T).

identifying the individual transitions.

The three highest-energy excitonic features in the summary plot of Fig. 3 are identified as the $1s \to 3p_+$ transitions (nearly degenerate as in the $2p_+$ case), and the $1s \to 3p_-$ $(m_j = \pm\frac{3}{2})$ transitions. These features can be seen in the lower trace of Fig. 2 at fields of 1.9 T $(3p_+)$, 2.8 T $[3p_-(-\frac{3}{2})]$, and 3.2 T $[3p_-(+\frac{3}{2})]$, respectively. Comparison of the energy differences between electron and hole CR's with those of the $1s \to 3p_-$ to $1s \to 3p_+$ transitions is in agreement with this assignment. At 84.2 cm^{-1} the two $1s \to 3p_-$ transitions are not resolved due to the small splitting in this low-field region.

In Fig. 3 the arrows at magnetic fields of 4 and 6 T display the relationship between the electron/hole-CR and the $1s \to 2p_\pm$ transition energies. The dashed arrows represent the energy differences between electron CR and the appropriate hole CR (from the data of Fig. 3). In the case of the $m_J = +\frac{3}{2}$ hole CR, a fit through the data points (parallel to the theoretically calculated line) was used. The solid arrows have the same length as the respective dashed arrows. With the bottom of the solid arrows placed at the respective $1s \to 2p_-$ transition, the top of the arrow "predicts" the position of the $1s \to 2p_+$ transition. As seen in the figure, the CR energy difference is very close to the $1s - 2p_\pm$ energy difference, and thus verifies the predicted symmetry-based relationship within experimental error for this sample. A quantitative comparison is given below.

A comparison of ODR data for the three samples is presented in Fig. 4 at two laser wavelengths. Figure 4(a) compares the ODR spectra at 118.8 μm. The systematic shift of the $1s$-$2p_+$ IET features to higher fields with increasing well width is apparent. The e-CR shows very little apparent dependence on well width over this range. In the field region between 6 and 9 T due to nonparabolicity, e-CR is expected to shift down in energy by 3–4 cm^{-1} between well widths of 20 and 12.5 nm. This corresponds to a shift in magnetic field
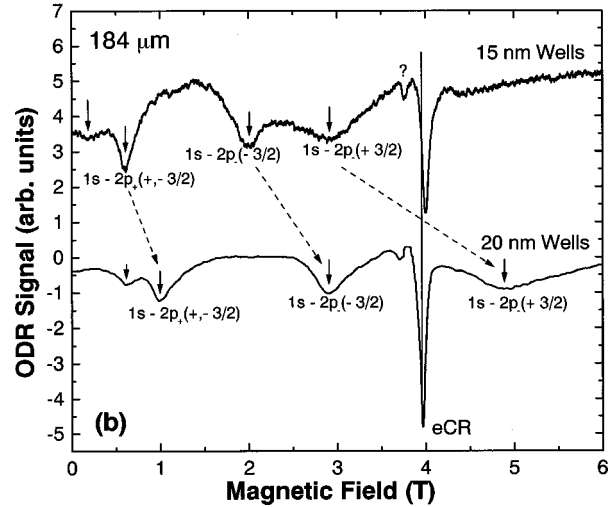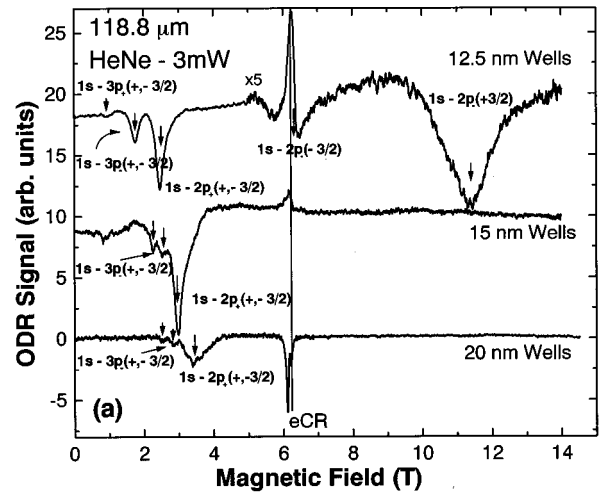

FIG. 4. (a) Comparison of ODR spectra for samples 1, 2, and 3 at a laser wavelength of 118.8 μm. The various transitions are labeled. (b) Similar comparison for samples 2 and 3 at a laser wavelength of 184 μm.

of 0.2–0.3 T, much greater than that observed. This apparent independence of e-CR on well width appears to result from localization of the electrons (particularly in sample 1) in lateral potential fluctuations. Localization leads to a blueshifted CR relative to the free carrier CR.[22] A clear indication of these effects is seen in samples 2 and 3. In sample 2 the e-CR is broad with an odd line shape (indicative of more than one line), and in sample 3 there are *two* sharp lines observed. The dominant peak occurs at about 6.12 T in the latter case, while a weaker peak occurs at about 6.22 T, the expected position for free carrier CR. In the summary data of Figs. 5 and 6, the higher-field peak is plotted. The relative strengths of the two peaks in samples 2 and 3 depend on the excitation intensity and the FIR laser intensity (carrier temperature) with the free carrier feature dominant at the higher intensities.

Figure 4(b) shows a similar comparison of ODR spectra for samples 2 and 3 at a laser wavelength of 184 μm. In this case all the IET's for sample 1 lie at higher photon energies at all fields and are not observable at 184 μm. Due to the small slope with magnetic field, the shifts to higher fields with increasing well width are even more dramatic. Qualita-
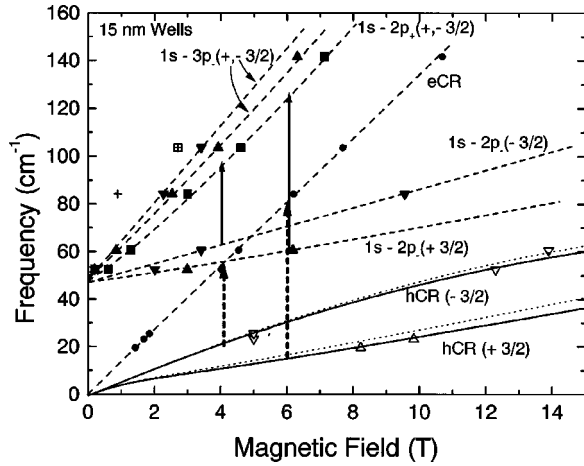
FIG. 5. Summary plot of the transition energies of the observed IET's and e-CR and h-CR's vs magnetic field for sample 2. Dashed lines are guides to the eye. Solid lines for the h-CR's are calculations described in the text with $x = 0.15$, and 60%/40% conduction-band/valence-band offsets; the dotted lines are the calculated h-CR's for the following set of Luttinger parameters: $\gamma_1 = 6.79$, $\gamma_2 = 1.92$, $\gamma_3 = 2.73$. The lower (dashed) arrows show the energy difference between e-CR and h-CR($+\frac{3}{2}$) (at 4 T), and h-CR ($-\frac{3}{2}$) (at 6 T). The upper (solid) arrows are the lower arrows vertically displaced to originate on the $1s \rightarrow 2p_-(+)$ transition (at 4 T) and the $1s \rightarrow 2p_-(-)$ transition (at 6 T).

tively, shifts to higher fields (lower energies) of the IET's with increasing well width are expected, since reduced confinement leads to smaller binding (and IET) energies at $B = 0$.

In Fig. 5 the ODR results from sample 2 (15-nm well width) are summarized for several FIR laser lines. The general features are very similar to those obtained for sample 1.
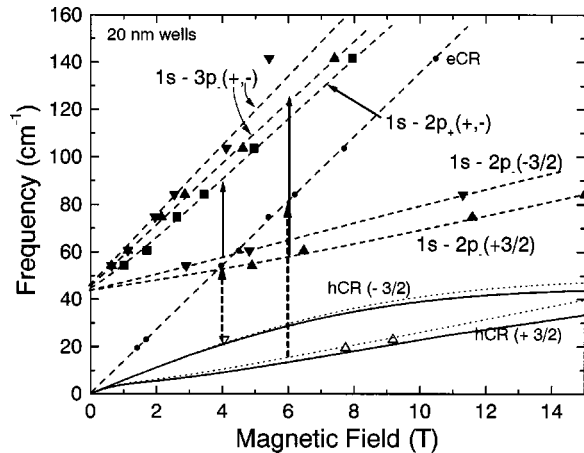

FIG. 6. Summary plot of the observed IET's and CR vs magnetic field for sample 3. Dashed lines are guides to the eye. Solid lines for the h-CR's are calculations described in the text with $x = 0.15$, and 60%/40% conduction-band/valence-band offsets; the dotted lines are the h-CR's for the following set of Luttinger parameters: $\gamma_1 = 6.79$, $\gamma_2 = 1.92$, $\gamma_3 = 2.73$. The lower (dashed) arrows show the energy difference between e-CR and h-CR($+\frac{3}{2}$) (at 4 T) and h-CR($-\frac{3}{2}$) (at 6 T). The upper (solid) arrows are the lower arrows vertically displaced to originate on the $1s \rightarrow 2p_-(+)$ transition (at 4 T) and the $1s \rightarrow 2p_-(-)$ transition (at 6 T).

At the longest wavelengths electron and hole CR are observed, while at shorter wavelengths electron CR and internal transitions of neutral, heavy-hole excitons are seen. As also shown in Figs. 4(a) and 4(b) the ODR features for the wider wells of sample 2 occur at systematically lower energies than the corresponding transitions from the narrower wells of sample 1. This general behavior is also apparent from a comparison of Fig. 5 with Fig. 3; over the entire field range investigated, corresponding IET's occur at lower energy in this plot than in the summary plot for sample 1. The extrapolated value of the $1s$-$2p$ energy at $B = 0$ is also substantially lower in sample 2 than in sample 1, as anticipated from the weaker confinement.

The hole cyclotron resonances for this sample are not as strong as those for sample 1, but resonances were nevertheless observed at several laser wavelengths. Within experimental error the data for the both the $m_J = -\frac{3}{2}$ and $+\frac{3}{2}$ holes agree with the calculation shown by the solid lines in Fig. 5. The agreement for the $+\frac{3}{2}$ CR is excellent. For comparison, a calculation with a different set of Luttinger parameters is also given in Fig. 5 by the dotted lines. The agreement for the $m_J = -\frac{3}{2}$ CR is still within experimental error, but with these Luttinger parameters, the calculated $+\frac{3}{2}$ h-CR lies systematically about 2 cm^{-1} higher than the experimental points. As can be seen from the arrows at 4 and 6 T in this figure, within experimental error the symmetry-derived relationship is obeyed for both the $m_J = +\frac{3}{2}$ and $-\frac{3}{2}$ transitions for this sample.

The ODR data for sample 3 (20-nm wells) are summarized in Fig. 6. Again, as seen in Figs. 4(a) and 4(b), the data for the various IET's for this sample are systematically lower in energy than the corresponding data of either sample 1 (Fig. 3) or sample 2 (Fig. 5). In this case h-CR for the $m_J = -\frac{3}{2}$ holes was observable only at one laser wavelength. It lies between 1 and 2 cm^{-1} *higher* than the calculated value with the Luttinger parameters used for the other samples. In this field region there is negligible difference between the calculated $-\frac{3}{2}$ h-CR for either set of Luttinger parameters. Again, the calculation with the alternative Luttinger parameters is shown by the dotted lines. The h-CR data for the $m_J = +\frac{3}{2}$, on the other hand, lies about 1–2 cm^{-1} higher in energy than the calculated line position with the original Luttinger parameters. In this case there is much better agreement with the calculation with the alternative Luttinger parameters. However, given the uncertainties in the well widths (± 5%) and the barrier compositions (± 0.03 in x), it is difficult to make a conclusive statement about which of the sets of Luttinger parameters provide the best agreement with the h-CR data. Both sets provide reasonably good agreement for the $-\frac{3}{2}$ h-CR for all samples, but neither set gives consistently good agreement for the $+\frac{3}{2}$ h-CR.

A check of the symmetry-derived relationship for this sample is again indicated by the arrows at 4 and 6 T. For the hole in the $m_J = -\frac{3}{2}$ state the agreement is quite good; on the other hand, for the hole in the $m_J = +\frac{3}{2}$ state the agreement is poor; $\hbar\omega_{ce}(-\frac{1}{2}) - \hbar\omega_{ch}(+\frac{3}{2})$ is greater than $E_{2p+}(-\frac{1}{2}) - E_{2p-}(+\frac{3}{2})$ by almost 10 cm^{-1}. This disagreement is discussed below.

The general behavior of the IET's with well width (confinement) is qualitatively as expected. The energies of particular IET's decrease at constant field as the well width is
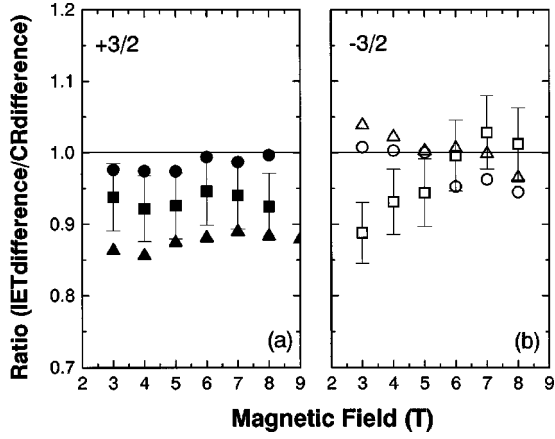
FIG. 7. Comparison of the ratio of the energy difference between e-CR and h-CR to the energy difference between the $1s$-$2p_+$ and $1s$-$2p_-$ transitions for the corresponding hole states: (a) $m_J = +\frac{3}{2}$, (b) $m_J = -\frac{3}{2}$. Samples 1, 2, and 3 are represented by squares, circles, and triangles, respectively.

increased. The data for the 12.5-nm wells of sample 1 extrapolate to a zero-field $1s \rightarrow 2p$ transition energy of about 60 cm^{-1}; the corresponding extrapolated zero-field energy for the 15-nm wells of sample 2 is about 48 cm^{-1}, and that of sample 3 is about 44 cm^{-1}, in reasonable agreement with calculations.[17]

To examine the symmetry-derived prediction relating the differences between e-CR and h-CR and the $1s$-$np_\pm$ energies more quantitatively, we plot the ratio of these energy differences (for the $2p$ states) to the corresponding cyclotron resonance energy differences as a function of magnetic field in Fig. 7 for all three samples (squares, circles, and triangles, correspond to sample 1, 2, and 3, respectively.). Figure 7(a) shows this comparison for the $1s \rightarrow 2p_\pm$ IET's for the $\left|-\frac{1}{2}, +\frac{3}{2}\right\rangle$ exciton (labeled by the hole spin) and the corresponding cyclotron resonance energy difference, $\hbar\omega_{ce}(-\frac{1}{2}) - \hbar\omega_{ch}(+\frac{3}{2})$. Figure 7(b) shows the same comparison for the $1s \rightarrow 2p_\pm$ IET's for the $\left|+\frac{1}{2}, -\frac{3}{2}\right\rangle$ exciton and the CR energy difference, $\hbar\omega_{ce}(+\frac{1}{2}) - \hbar\omega_{ch}(-\frac{3}{2})$. Generally, the experimental values agree with prediction reasonably well for the $m_J = -\frac{3}{2}$ hole state; the ratios cluster around a value of 1 to better than 10%. The agreement is best for the 15-nm well width of sample 2 and agreement is also very good for the 20-nm well-width sample. The poorest agreement is for the narrowest well-width sample (sample 1) at low magnetic fields. Given the measurement uncertainties (at low fields the estimated error is greater than $\pm$5%) this agreement is considered satisfactory. On the other hand, for the $m_J = +\frac{3}{2}$ state there appear to be systematic errors. Although there is less scatter in the data for individual samples, all the ratios are systematically low, with the best agreement (again) for the 15-nm well-width sample, and the largest discrepancy (close

to 15%) occurring for the 20-nm well-width sample. For this well width, the mixing between the "light" ($m_J = \pm\frac{1}{2}$) and "heavy"-hole ($m_J = \pm\frac{3}{2}$) Landau levels is very large, as evidenced in Fig. 6 by the large curvature in the $m_J = -\frac{3}{2}$ hole CR energy vs B. Increased mixing of these states is concomitant with the increasing importance of the warping (noncylindrically symmetric) terms in the Hamiltonian, which have been neglected, and which break the symmetry leading to the simple relationship. Part of the systematic decrease of the ratio for the 12.5-nm sample is likely due to an overestimate of the e-CR energy, and a concomitant overestimate of the CR energy differences. As discussed above, the observed e-CR occurs systematically 2–3 cm^{-1} higher than free electron CR at this well width due to localization.[23] In the wider well samples two e-CR lines are distinguished [Figs. 4(a) and 4(b)] and the data used in the analysis are the positions of the higher-field (lower energy) free carrier CR.

The observation of only one resolved $1s \rightarrow 2p_+$ line in all three samples, even though there are two energetically distinguishable magnetoexcitons in PL, $\left|\frac{1}{2}, -\frac{3}{2}\right\rangle$ and $\left|-\frac{1}{2}, +\frac{3}{2}\right\rangle$, results from the fact that the $1s \rightarrow 2p_+$ transitions correspond to promotion of the electron from a state associated with the lowest LL to a state associated with the first LL, as discussed in Sec. II. Since the energy difference between e-CR$(+\frac{1}{2})$ and e-CR$(-\frac{1}{2})$ is very small in this field range, the two corresponding allowed $1s \rightarrow 2p_+$ features are not distinguishable. On the other hand, the $1s \rightarrow 2p_-$ transitions from the two different excitons correspond to promoting the hole from a state associated with the lowest hole LL to a state associated with the first hole LL. Since there is a large splitting between the $\pm\frac{3}{2}$ h-CR's (see Fig. 1), there is a correspondingly large (measurable) energy separation between the two $1s \rightarrow 2p_-$ IET's.

V. SUMMARY AND CONCLUSIONS

The high sensitivity and general utility of the ODR technique are clear from the present results. The simultaneous detection of e-CR, $m_J = \pm\frac{3}{2}$ h-CR's, and several internal excitonic transitions has allowed a clear observation of the consequences of the symmetry for this electron-hole system. The predicted relationship between the energy differences between the np_+ and np_- internal transitions and the energy differences between e-CR and the $m_J = \pm\frac{3}{2}$ h-CR's has been verified. Calculations of the h-CR energies vs B are generally in good agreement with the measurements.

ACKNOWLEDGMENTS

[1] F. Ancilotto, A. Fasolino, and J. C. Maan, Phys. Rev. B **38**, 1788 (1988).

[2] R. C. Miller and D. A. Kleinman, J. Lumin. **30**, 520 (1985).

[3] G. E. W. Bauer and T. Ando, Phys. Rev. B **38**, 6015 (1988).

[4] The solutions of the Schrödinger equation for the internal motion with center-of-mass momentum set equal to zero comprise a set of discrete states that evolve continuously from the usual 3D, low-field hydrogenic states with increasing confinement and magnetic field. In this sense they can be labeled with the usual 3D, $B=0$ quantum numbers even for strong confinement and high magnetic fields. States labeled nlm in the quasi-2D, high-field situation track continuously to this 3D state as the well width is increased to infinity and the field is decreased to zero. [See, e.g., J.-P. Cheng and B. D. McCombe, Phys. Rev. B **42**, 7626 (1990).] This labeling has become common practice in the literature.

[5] L. Viña, G. E. W. Bauer, M. Potemski, J. C. Maan, E. E. Mendez, and W. I. Wang, Phys. Rev. B **41**, 10 767 (1990).

[6] Internal transitions of photoexcited excitons in the GaAs/AlAs system by photoinduced absorption spectroscopy have been reported by C. C. Hodge, C. C. Phillips, M. S. Skolnick, G. W. Smith, C. R. Whitehouse, P. Dawson, and C. T. Foxon, Phys. Rev. B **41**, 12 319 (1990); excitons have also been studied in bulk Ge and Si by similar techniques, e.g., E. M. Gershenzon, G. N. Gol'tsman, and N. G. Ptitsina, Zh. Eksp. Teor. Fiz. **70**, 224 (1976) [Sov. Phys. JETP **43**, 116 (1976)] and D. Labrie, M. L. W. Thewalt, I. J. Booth, and G. Kirczenow, Phys. Rev. Lett. **61**, 1882 (1988). The long lifetimes for these indirect gap systems permit a large exciton density to be excited at relatively low excitation intensities.

[7] A. B. Dzyubenko, Pis'ma, Zh. Eksp. Teor. Fiz. **66**, 588 (1997) [JETP Lett. **66**, 617 (1997)]; H. A. Nickel, G. S. Herold, M. S. Salib, G. Kioseoglou, A. Petrou, B. D. McCombe, and D. Broido, Physica B **249–251**, 598 (1998).

[8] G. Finkelstein, H. Shtrikman, and I. Bar-Joseph, Phys. Rev. B **53**, R1709 (1996).

[9] D. Gekhtman, E. Cohen, Azra Ron, and L. N. Pfeiffer, Phys. Rev. B **54**, 10 320 (1996).

[10] H. A. Nickel, G. S. Herold, T. Yeo, G. Kioseoglou, Z. X. Jiang, B. D. McCombe, A. Petrou, D. Broido, and W. Schaff, Phys. Status Solidi B **210**, 341 (1998); A. B. Dzyubenko and A. Yu. Sivachenko, Phys. Rev. Lett. **84**, 4429 (2000).

[11] M. G. Wright, N. Ahmed, A. Koohian, K. Mitchell, G. R. Johnson, B. C. Cavenett, C. R. Pidgeon, C. R. Stanley, and A. H. Kean, Semicond. Sci. Technol. **5**, 438 (1990); N. Ahmed, I. R. Agool, M. G. Wright, K. Mitchell, A. Koohian, S. J. A. Adams, C. R. Pidgeon, B. C. Cavenett, C. R. Stanley, and A. H. Kean, *ibid.* **7**, 357 (1992).

[12] J. G. Michels, R. J. Warburton, R. J. Nicholas, and C. R. Stanley, Semicond. Sci. Technol. **9**, 198 (1994).

[13] A. Moll, C. Wetzel, B. K. Meyer, P. Omling, and F. Scholz, Phys. Rev. B **45**, 1504 (1992).

[14] S. J. Gubarev, A. A. Dremin, I. V. Kukushkin, A. V. Malyavkin, M. G. Tyazhlov, and K. von Klitzing, Pis'ma Zh. Eksp. Teor. Fiz. **54**, 361 (1991) [JETP Lett. **54**, 355 (1991)].

[15] R. J. Warburton, J. G. Michels, R. J. Nicholas, J. J. Harris, and C. T. Foxon, Phys. Rev. B **46**, 13 394 (1992).

[16] J. Kono, S. T. Lee, M. S. Salib, G. S. Herold, A. Petrou, and B. D. McCombe, Phys. Rev. B **52**, R8654 (1995); G. S. Herold, H. A. Nickel, J. G. Tischler, B. A. Weinstein, and B. D. McCombe, Physica E (Amsterdam) **2**, 39 (1997).

[17] M. S. Salib, H. A. Nickel, G. S. Herold, A. Petrou, B. D. McCombe, R. Chen, K. K. Bajaj, and W. Schaff, Phys. Rev. Lett. **77**, 1135 (1996).

[18] J. Černe, J. Kono, M. S. Sherwin, M. Sundaram, A. C. Gossard, and G. E. W. Bauer, Phys. Rev. Lett. **77**, 1131 (1996).

[19] J. Kono, M. Y. Su, J. Černe, M. S. Sherwin, S. J. Allen, Jr., T. Inoshita, T. Noda, and H. Sakaki, Physica B **249–251**, 527 (1998).

[20] R. Romestain and C. Weisbuch, Phys. Rev. Lett. **45**, 2067 (1980).

[21] I. V. Lerner and Yu. E. Lozovic, Zh. Eksp. Teor. Fiz. **78**, 1167 (1980) [Sov. Phys. JETP **51**, 588 (1980)].

[22] G. Kioseoglou, H. D. Cheong, T. M. Yeo, H. A. Nickel, A. Petrou, B. D. McCombe, A. Yu. Sivachenko, and A. B. Dzyubenko, and W. Schaff, Phys. Rev. B **61**, 5556 (2000).

[23] For a number of similar MQW samples at 4.2 K we have observed small blueshifts of the observed e-CR from the free carrier e-CR in magnetotransmission measurements at fields between 6 and 9 T; the shifts for 20-nm wells were 1–2 cm^{-1}. In these samples, which were lightly doped with donors in the wells (7×10^9 cm^{-2}) or in the barriers (2×10^{10} cm^{-2}) or in both wells and barriers, the observed e-CR shifted down in energy by 1–2 cm^{-1} as the temperature was raised to 10–15 K. The position of e-CR at the elevated temperatures agrees with the predicted position calculated with the nonparabolicity of the conduction band included, and also with the position observed for more heavily modulation-doped samples. These effects are attributed to localization of the electrons in long-range, lateral potential fluctuations: see, e.g., J.-P. Cheng and B. D. McCombe, Phys. Rev. B **44**, 3070 (1991); U. Merkt, Phys. Rev. Lett. **76**, 1134 (1996).